# Frequency-Domain Identification Algorithms for Servo Systems With Friction

Yung-Yaw Chen, *Member, IEEE*, Pai-Yi Huang, and Jia-Yush Yen

***Abstract*—Mechanical devices usually come with undesirable nonlinearities, such as friction, backlashes, and saturations. Under the assumption of linear systems, the commonly seen identification schemes utilize sinusoidal excitation signals for parameter identification. However, the data needed for identification are unavoidably distorted by the aforementioned nonlinearities and the identification result may not be satisfactory. In this paper, binary test signals are used to perform identification, thus simplifying the behavior of friction. An identification method based on the difference of binary multifrequency excitation signals is proposed. The modified identification algorithm does not suffer from the problem of nonlinear distortions in the signal shape and is able to determine the nonlinear friction such that an accurate servo system model can be derived. A high-precision ball–screw table with asymmetric friction is identified as a test plant for this approach. The results prove that the method can be used very successfully.**

***Index Terms*—Binary multifrequency signal, frequency domain, friction compensation, identification algorithms, system identification.**

## I. Introduction

THE PURPOSE of system identifications is to extract mathematical models from physical systems. A properly identified model can help us understand the details of a system and estimate its behaviors under specified inputs by means of computer simulation. Nowadays, the increasing need for precision machining and processing of semiconductors, optoelectronic elements, and high-density magnetic memory devices has increased the demand for high-accuracy machining at the level of submicrometers. To achieve such precision, accurate system models are mandated.

A general system identification problem, as defined by Zadeh [1], is characterized by three components: a class of models, a class of input signals and an identification criterion. The class of models should be appropriate and the set of signals should have the property of persistent excitations relative to the class of models. A recursive criterion is usually adopted to extract target parameters from the I/O data. Successful system identification, therefore, depends on careful consideration of the previous entities.

Manuscript received October 13, 2000; revised August 28, 2001. Manuscript received in final form April 11, 2002. Recommended by Associate Editor K. Kozlowski. This work is supported by National Science Council, Taiwan, R.O.C., under Grant NSC 89-2213-E-002-090.

Y.-Y. Chen is with the Department of Electrical Engineering, National Taiwan University, Taipei, Taiwan, R.O.C. (e-mail: yychen@cc.ee.ntu.edu.tw).

P.-Y. Huang is with the ASUSTek Computer, Inc., Taipei, Taiwan, R.O.C. (e-mail: Pai-Yi_huang@asus.com.tw).

J.-Y. Yen is with the Department of Mechanical Engineering, National Taiwan University, Taipei, Taiwan, R.O.C. (e-mail: jyen@ccms.ntu.edu.tw).

Publisher Item Identifier 10.1109/TCST.2002.801804.

Generally, there are two major categories of system models. One is the time-domain formulation models and the other one is the frequency-domain formulation models. Although modern control theories employed in state–space representations are widely accepted by control communities, quite a few system specifications are still expressed in terms of frequency-domain parameters, e.g., the frequency specifications of a CD-ROM pickup head. In real-world applications, frequency-domain methods are still widely applied by conventional engineers in system modeling.

It is known to all control engineers that classical theories of frequency response only apply to linear systems [2]. Most nonlinear systems have to be linearized around a specific operating point such that a linear model can be derived. Typical identification procedures include spectrum estimation techniques based on covariance and Fourier transform analyses [3]. The existence of nonlinearity, such as friction, backlashes, and saturations, in practical systems is usually not modeled and is ignored in the identification process. As a result, the almost always unavoidable nonlinearities jeopardize the validity of the identification results such that a precise description of the system becomes very hard to obtain.

Among the commonly observed nonlinearities, friction is regarded as one of the most significant factors and has been extensively discussed. Studies on system friction have mostly focused on its behaviors, such as static friction, dynamic friction, the Stribeck phenomena, and friction memories [4]–[7]. A simplified plant model of a one-pole system is usually adopted to reduce the complexity of the friction identification problem as in [8]–[10]. Most existing methods in the literature are time-domain online identification methods which employ adaptive algorithms. Friction parameters are derived based on knowledge of the system and complicated mathematical theories. More recently, an evolutionary programming approach has been proposed [11] to deal with the same problem. This method can identify the system friction by formulating the identification task as an optimization problem. Unlike the gradient descent-based approach, evolutionary programming offers a better chance in finding global optimal solutions. However, its speed of convergence is rather slow compared with the conventional search methods.

In this paper, a novel frequency-domain system identification method is proposed for systems with friction. The major advantage of this approach is its application of differential binary signals to system excitations, by means of which the commonly seen nonlinear distortions due to friction can be successfully decoupled. Hence, an accurate model of the plant and the associated friction can be obtained. The proposed method has

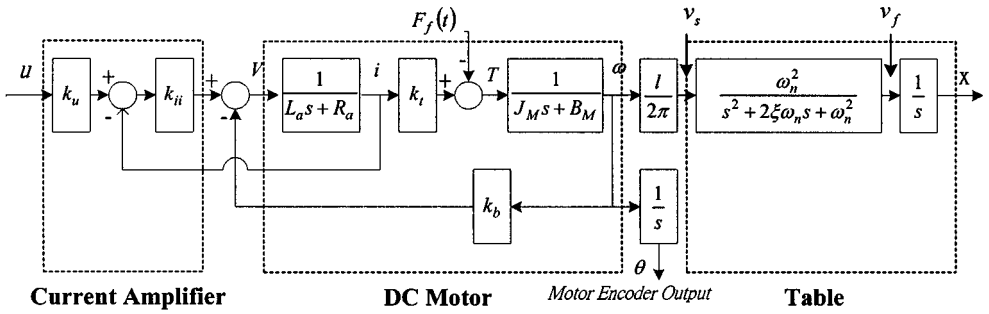


Fig. 1. Block diagram of a servo system.

been formulated and applied to a precision ball–screw table with excellent results.

The organization of this paper is as follows. Section II will discuss the mathematical formulation and motivation of the proposed method. Section III will present the identification procedures in detail. Section IV will give identification results based on two numerical examples. Section V will present the experimental setup and the excellent identification results. Finally, a conclusion will be given in Section VI.

## II. Servo Systems With Frictions

It is common practice to assume linearity of the target system in frequency-domain identification. But most real-world systems are nonlinear in nature, so the linearity assumption may significantly reduce the accuracy of the identified model. In this section, we shall provide a detailed description of a servo system and its associated nonlinear friction so that a mathematical model can be established for the purpose of further discussion. Then, the ideas that form the basis of our identification approach will be fully explained.

### A. Model of Servo Systems

A typical servo system usually consists of a plant (such as a slider table), an actuator (such as a dc motor), and some driving circuits as shown in the block diagram in Fig. 1.

The slider table is modeled as a second-order transfer function and is driven by a dc motor that is also modeled as a second-order system. The position of the slider table can be measured by means of a motor encoder or directly by means of a position sensor (such as an optical position sensor) attached to the table. To obtain semiposition feedback, the rotating angle $\theta$ of the motor is derived by transforming the encoder readings into position readings by multiplying by a constant $l/2\pi$, where $l$ is the pitch of the ball–screw driving the slider table. Since the table position is not directly read out, there are always errors on the order of several micrometers in the position readings which comprise semiposition feedback.

The function of the current amplifier is to keep the motor armature current $i$ proportional to the input command $u$, independent of the motor back electromotive force (EMF) $k_b \cdot \omega$. The gain $k_{ii}$ is usually very large and in the dynamic range of the mechanics, the current loop gain can be considered as a constant $k_i$; therefore, the transfer function from input $u$ to the equivalent transversal speed $v_s$ of the motor axis is written as

$$G_{uv_s} = \frac{l}{2\pi} \cdot \frac{k_i k_u}{J_M s + B_M}. \tag{1}$$

To increase resolution to the submicrometer level, full-position feedback is utilized by directly measuring the table position. The transfer function for full position feedback can be described by

$$G_{uv_f} = \frac{l}{2\pi} \cdot \frac{k_i k_u}{J_M s + B_M} \cdot \frac{\omega_n^2}{(s^2 + 2\xi\omega_n s + \omega_n^2)}. \tag{2}$$

By letting $M = 2\pi J_M / l k_i k_u$ and $B = 2\pi B_M / l k_i k_u$, transfer function (1) can be simplified to obtain

$$G_{uv_s} = \frac{1}{(Ms + B)}. \tag{3}$$

In addition, (2) can be simplified to obtain

$$G_{uv_f} = \frac{1}{Ms + B} \cdot \frac{\omega_n^2}{(s^2 + 2\xi\omega_n s + \omega_n^2)}. \tag{4}$$

Most of the previous studies on friction with dc servo systems as in [8] and [9] have started with a system model like that in (3). By adding the friction term (as shown in Fig. 1), we can obtain the dynamical equation

$$M\frac{dv}{dt} + Bv = u(t) - F_f(v) \tag{5}$$

where $v$ is the velocity variable and $F_f(t)$ is the friction force. Based on the previous discussion, we can also describe the full position feedback system described in (4) by the block diagram in Fig. 2.

### B. Model of Friction

In general, the most significant friction components in a servo system are the static friction and the Coulomb friction. The friction force in (5), $F_f(t)$, is usually modeled as shown in Fig. 3 as asymmetric Coulomb friction. $F_s^+$ and $F_s^-$ are the static friction and the $F_c^+$ and $F_c^-$ are the Coulomb friction associated with positive and negative velocities, respectively. Thus, the friction force can be formulated mathematically as in the following equations: when $|\dot{x}| > 0$ (called slipping)

$$F_f(\dot{x}) = F_c^{\mathrm{sgn}(\dot{x})} \cdot \mathrm{sgn}(\dot{x}) \tag{6}$$

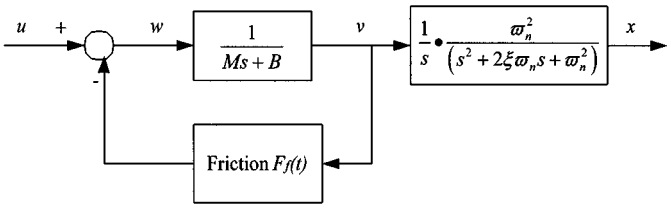


Fig. 2. Simplified system block diagram.

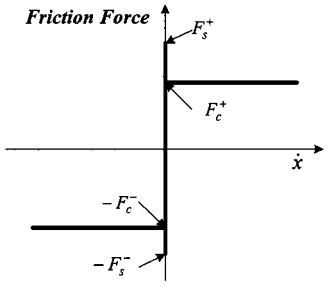


Fig. 3. Relationship between the friction force and the velocity of $x$.

when $\dot{x} = 0$ (called sticking)

$$F_f(\dot{x}=0) = \begin{cases} u, & \text{for } -F_s^- \le u \le F_s^+ \\ F_s^+ \text{ or } F_s^-, & \text{depending on direction of } u \end{cases}. \quad (7)$$

Viscous friction depending on the velocity is not included in this friction model because the effects of such friction will be combined into the damping behaviors of the servo system.

### C. Decomposition of Servo Systems With Friction

Consider a plant consisting of servo systems as shown in Fig. 4(a) and one main friction element existing in the systems. In order to identify the plant, input $u$ is applied and output $v$ is measured accordingly to determine the I/O data pairs. The quality of the derived model depends on the specified input $u$, the measuring conditions of output $v$ and the identification scheme. In the conventional frequency-domain identification methods based on covariance analysis and Fourier transform, the plants to be identified are always assumed to be linear.

However, this assumption is almost always invalid due to the existence of friction. From (5), it can be seen that the friction force can be treated as a nonlinear negative feedback term from the output velocity. That is, the plant shown in Fig. 4(a) can be decomposed into a linear block $G(s)$ with a nonlinear feedback element as shown in Fig. 4(b). The linear block in the feedforward path describes the system dynamics and the nonlinear block in the feedback path describes the friction with $w$ being the input to the linear block.

From Fig. 4(b), it is obvious that $w$ and $v$ are the input and output of the linear block, respectively. Existing methods are quite useful if $w$ and $v$ can be used as the I/O pairs for the purpose of identification. However, instead of having $(w, v)$ pairs, we inevitably have $(u, v)$ pairs. It is also generally true that $w$ is very different from $u$ due to nonlinear feedback distortions.

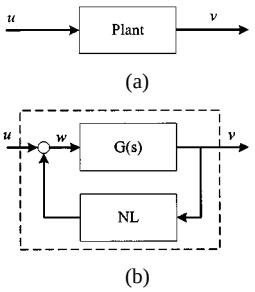


Fig. 4. (a) General servo plant. (b) Decomposition of the plant into linear and nonlinear blocks.

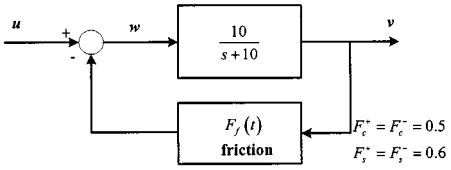


Fig. 5. Simple servo system with friction.

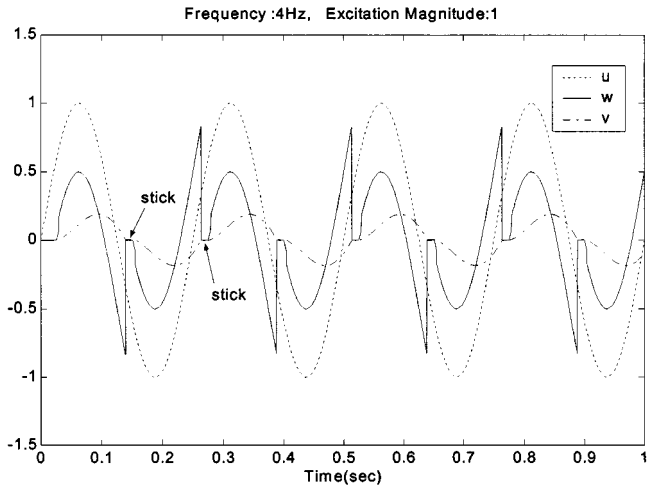


Fig. 6. System responses with sinusoidal input excitations ($u$: dashed, $v$: dash-dot, $w$: solid).

## III. New Ideas About System Identification With Friction

Let us consider the plant shown in Fig. 5 with static and Coulomb friction. The two types of friction are assumed to be different constants according to their different directions. A simulation result is shown in Fig. 6 with a pure sinusoidal input $u$. The dotted line is the input signal $u$, the dash-dot line is the velocity trace $v$, and the solid line is the input $w$ that is seen by the linear block. In this simulation, the input signal is rather slow with respect to the system dynamics. As a result, we can see the stick-slip phenomena that is commonly found in mechanical systems and $u$ and $w$ are quite different.

### A. Response With Square-Wave Input

Because the actual input to the linear block $w$ is quite different from the input signal $u$ used in identification, the linear frequency-domain identification methods are not able to provide a satisfactory model of the linear block or the entire plant.

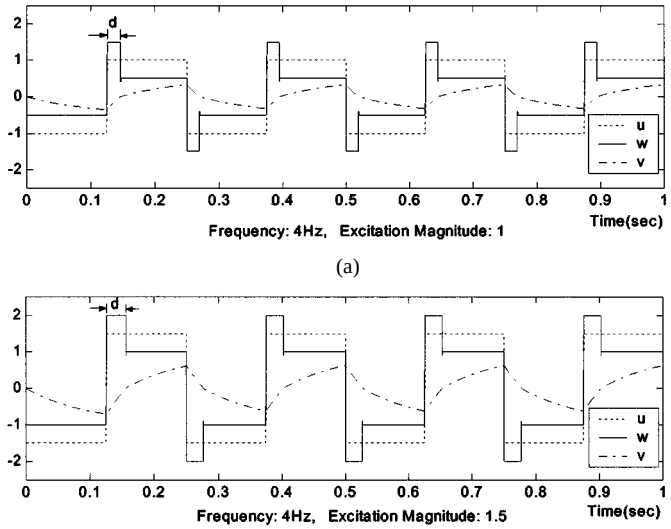


Fig. 7. Responses (a) with square-wave input and an excitation magnitude of 1; (b) with square-wave input and an excitation magnitude of 1.5. ($u$: dashed, $v$: dash-dot, $w$: solid).

Moreover, it can be observed that the difference between $u$ and $w$ is mostly contributed by the stick-slip caused by friction. Therefore, if we choose for $u$ a magnitude larger than the total frictional force, then the friction behavior will be simplified and the stick phenomenon will be eliminated because there will be a nonzero acceleration force in the system at all times [12].

Based on this assumption, it seems logical to choose square waves for input signals and to set the magnitude of the chosen square waves larger than the static friction $F_s^+$ and $F_s^-$ so that the friction will be in the slip mode. In Fig. 7, the dotted line represents the input $u$ and the solid line denotes the input to the linear block $w$. At first glance, the input to the linear block $w$ appears to be similar to a square wave except for the overshoots in each direction change of input $u$. The magnitude of each overshoot is equal to the span of the Coulomb friction, $F_c^+ + F_c^-$, as shown in Fig. 7(a). The overshoots are caused by changes in the direction of the driven force. With the velocity of the system continuing in the same direction, the friction force continues in the same direction as the driven force until the velocity of the system changes direction. The duration of the overshoot is denoted by $d$. It can also be observed that when the input signal $u$ increases from 1 to 1.5 as shown in Fig. 7(b) the duration $d$ also increases.

### *B. Response With Differential Square Wave Input*

From Fig. 4(b), assuming that $u_1$ and $u_2$ are two different input signals, $v_1$ and $v_2$ are the corresponding outputs, and $w_1$ and $w_2$ are the inputs to the linear block, respectively. Then, we have a linear mapping between the input of the linear block and the output, i.e.,

$$w_1 \rightarrow v_1 \text{ and } w_2 \rightarrow v_2. \tag{8}$$

Based on the fact that $(w, v)$ is a linear mapping, we have

$$w_1 - w_2 \rightarrow v_1 - v_2. \tag{9}$$

Let us consider the inputs and the responses shown in Fig. 7(a) and (b). The difference between the square wave inputs $u$ is shown in Fig. 8(a) and the difference between the inputs of the linear block $w$ is shown in Fig. 8(b). It can be seen that they are very similar except for the small glitches caused by the overshoots. Moreover, it will be shown in Section III-C that the glitches will become even smaller as the input magnitudes increase as shown in Fig. 8(c).

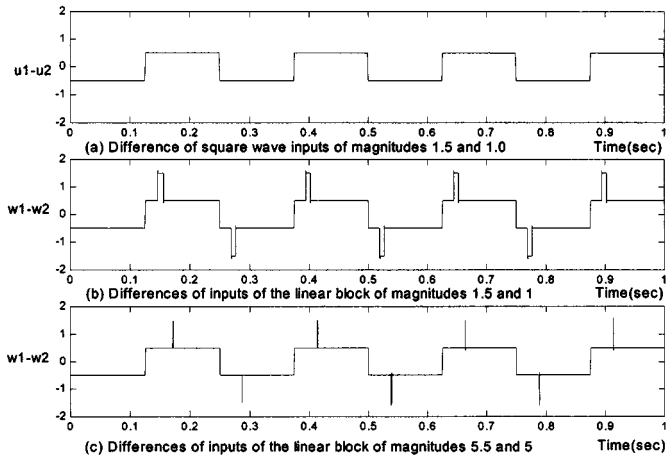


Fig. 8. (a) Difference between the square-wave inputs of magnitude 1.5 and 1.0. (b) Difference between the inputs of the linear block of magnitude 1.5 and 1.0. (c) Difference between the inputs of the linear block of magnitude 5.5 and 5.0.

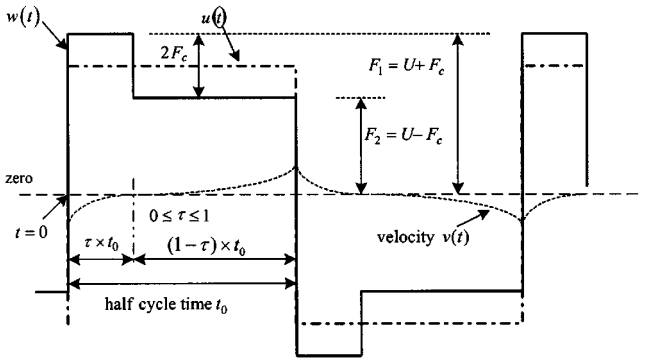


Fig. 9. Definitions used in the dimensional analysis.

### *C. Mathematical Analysis*

The steady-state relations of the overshoot duration, excitation frequency, and excitation magnitude for the square-wave response are investigated in the following dimensional analysis.

For a square-wave input to the plant shown in Fig. 5, the corresponding input to the linear block and the output would have the waveform shown in Fig. 6. One period of response is shown in Fig. 9, with $t = 0$ defined as the point of transition of the response from negative to positive.

First, scaling the time coordinate by a factor of $1/\beta$ gives the dimensionless time $t^*$, i.e.,

$$t^* = \beta \cdot t = \frac{1}{t_0} \cdot t \tag{10}$$

where the time scaling factor $\beta$ is defined as $1/t_0$ and $t_0$ is the half cycle time of the given square excitations.

If we choose a magnitude larger than the static friction for the square wave input, then the system friction will always be in the slip mode and the input to the linear block ($w$) will be

a piecewise constant. At $t = 0$, the output velocity will not be able to catch up instantly and the friction force will continue in the same direction as the input. As a result, the input to the linear block will become $F_1 = U + F_c$, where $U$ represents the magnitude of $u(t^*)$.

For the system described by (5), the system dynamics can be reformulated with the dimensionless time variable $t^*$ as

$$\dot{v}(t^*) + a \cdot v(t^*) = F(t^*) \tag{11}$$

where $a = B/M\beta$, $F(t^*) = (u(t^*) - F_c \cdot \text{sgn}(v))/M\beta$.

The solution of (11) with the unit square wave input in $[0, \tau]$ is

$$v(t^*) = \frac{F(t^*)}{a}\left(1 - e^{-a \cdot t^*}\right) + v(0) \cdot e^{-a \cdot t^*} \tag{12}$$

where $\tau$ denotes the time when the output velocity becomes zero. In order to solve $v(0)$, (12) can be solved at $t^* = \tau$

$$\frac{F_1}{B}\left(1 - e^{-a \cdot \tau}\right) + v(0) \cdot e^{-a \cdot \tau} = 0 \tag{13}$$

$$\Rightarrow v(0) = -\frac{F_1(1 - e^{-a \cdot \tau})}{B \cdot e^{-a \cdot \tau}}. \tag{14}$$

Next, the input to the linear block becomes $F_2 = U - F_c$ after $t^* = \tau$, when the velocity changes direction. Moreover, the relation $v(0) = -v(1)$ must hold for the steady-state response and the following equation can be derived:

$$\frac{F_2}{B}\left(1 - e^{-a \cdot (1-\tau)}\right) + 0 \cdot e^{-a \cdot (1-\tau)} = \frac{F_1(1 - e^{-a \cdot \tau})}{B \cdot e^{-a \cdot \tau}}. \tag{15}$$

After some manipulations of (15), we have

$$\frac{e^{-a \cdot \tau} - e^{-a}}{1 - e^{-a \cdot \tau}} = \frac{F_1}{F_2} = 1 + \Delta \tag{16}$$

where $\Delta > 0$ because $F_1 > F_2$. The percentage overshoot duration $\tau$ can be described by

$$\tau = \frac{-\log\left(\frac{1 + \Delta + e^{-a}}{2 + \Delta}\right)}{a}. \tag{17}$$

Let us consider the system shown in Fig. 5 as an example. The percentage overshoot duration $\tau$ is calculated using different values of the excitation magnitude as well as different excitation frequencies. The result is shown in Fig. 10. It can be seen that the changing rate of the percentage of the overshoot duration decreases as the excitation magnitude increases. As a result, the difference between the inputs to the linear block (e.g., $w_1 - w_2$) becomes almost the same as the difference between the square wave inputs as shown in Fig. 8(b) and (c) if a larger excitation magnitude is chosen. For example, a higher magnitude (5.5–5) will produce better results than a lower magnitude (1.5–1) as shown in Fig. 8. Moreover, it is shown in Fig. 10 that the percentage of the overshoot duration cannot exceed 50%.

### D. Novel Approach to System Identification With Friction

From the above discussion, it is clear from Figs. 8 and 9 that $(u_1 - u_2)$ can be almost identical to $(w_1 - w_2)$ if $u_1$ and $u_2$ are properly chosen. By taking $(u_1 - u_2)$ and $(v_1 - v_2)$ as the I/O pairs, which are equivalent to the I/O pairs $(w_1 - w_2)$ and $(v_1 - v_2)$, the linear block of the target system shown in Fig. 4 can be easily identified using a number of identification schemes.

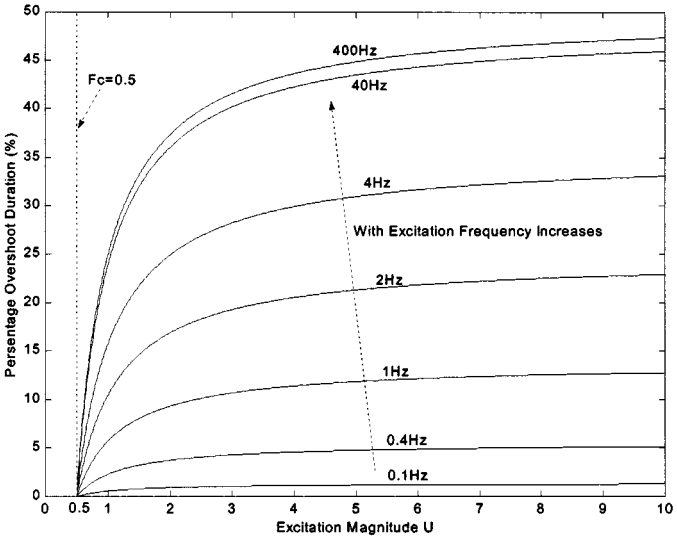


Fig. 10. Relationship between the percentage overshoot duration ($\tau$) and the excitation magnitude $U$; the minimum excitation magnitude is 0.5 because the value of the static friction is assumed to be 0.5 in this example.

## IV. System Identification by Differential Binary Excitation

In this section, the method of system identification by differential binary excitation (SIDBE) for proper identification of servo systems with friction will be described and summarized. We will start with the issue of input excitation design. Then, the identification algorithm will be discussed. Furthermore, the Coulomb friction will be derived after the transfer function of the linear block is identified. Finally, the identification procedures will be given.

### A. Design of Input Excitation

In conventional frequency-domain analysis, a single-frequency sinusoidal input is usually used to identify system behaviors. By gradually stepping through the desired frequency range, the frequency characteristics of the system can be gathered point by point. The process is simple but rather time-consuming. Alternatively, multifrequency excitation that contains all the frequencies of interest can be constructed and applied to the system so that the frequency response can be acquired in one pass.

The method for generating multifrequency binary excitations can be found in the work of ven den Bos and Krol [13] and Paehlike and Rake [14], where a multifrequency binary excitation is generated from an optimized multifrequency sinusoidal waveform through a comparator in time domain.

The choice of binary excitation is another important issue [15]. In a linear system, the linear block distorts the input signal only with respect to its magnitude and phase; the frequency components of the input signal remain unchanged. Unfortunately, the situation is quite different in nonlinear cases. A pure sinusoidal signal injected into a nonlinear block may produce responses at the fundamental frequency (i.e., the input frequency) and its entire harmonics. Furthermore, if multifrequency inputs are applied, not only will harmonics be produced, but intermodulation components at the frequencies

of the sums and differences of the fundamental frequency and their harmonics will also be generated. These harmonics could occur at the fundamental input frequencies, resulting in superposition of the harmonics on the fundamental response components and causing corruption of the frequency response. A technique devised by Mueller *et al.* [16] to improve the identification result is to select noninterfering input frequencies with properly scaled input magnitudes. In our design, we choose frequency components of prime-number multiples of the fundamental frequency to reduce the frequency distortions caused by nonlinear friction.

### *B. Maximum Likelihood System Identification*

In this paper, the estimator for linear systems (ELiS) devised by Kollár [17], which is based on maximum likelihood, is used to estimate system parameters. Based on band-limited measurements of input and output signals, ELiS can directly identify $s$-domain transfer functions. Consider the following system equation from input $u$ to output $v$:

$$v_i = \frac{N(\Omega_i, P)}{D(\Omega_i, P)} \cdot u_i = H(\Omega_i, P) \cdot u_i \tag{18}$$

where $N$ and $D$ are polynomials of $\Omega_i$, $\Omega_k = s_k = j\omega_k$ in the $s$-domain and $P = [a_0 a_1 \cdots a_d b_0 b_1 \cdots b_n]$ is the unknown parameter set to be identified. Assume that the measurements are made at angular frequencies $\omega_k$, $k = 1 \cdots F$ and that the measured complex input and output amplitudes are $u_{mk}$ and $v_{mk}$, respectively. The basic equation can be written as

$$v_{mk} = H(\Omega_k, P)(u_{mk} - N_{uk}) + N_{vk}. \tag{19}$$

The cost function for correrated I/O noise maximum likelihood estimation is defined as

$$C(P) = \frac{1}{2}\sum_{i=1}^{N} \frac{\left|e^{-j\omega_i T_d} N(\Omega_k, P) u_{mk} - D(\Omega_k, P) v_{mk}\right|^2}{\sigma_{vk}^2 |D(\Omega_k, P)|^2 + \sigma_{uk}^2 |D(\Omega_k, P)|^2 - 2\text{real}\{CND_k\}} \tag{20}$$

with

$$CND_k = c_{uvk} e^{-j\omega_k T_d} \overline{N(\Omega_k, P)} D(\Omega_k, P) \tag{21}$$

and

$$c_{uvk} = 0.5\text{cov}\{N_{uk}, N_{vk}\} = 0.5E\{\overline{N_{uk}} N_{vk}\}. \tag{22}$$

where $E\{\}$ stands for the statistical expectation value. The overall objective of estimation is to find the set $P$ that can minimize the cost function in (20).

In our proposed SIDBE, the time-domain signals of the difference between inputs $u_1 - u_2$ and the difference between outputs $v_1 - v_2$ are supposedly used as the I/O pair for system identification. However, in order to reduce the effect of noises, the time-domain I/O data are transformed into the frequency domain in advance and the differences are derived only at those frequencies that are of interest.

In ELiS, as explained by Pintelon and Schoukens [18], the properties of the estimate are robust. Furthermore, ELiS converges very well even for rather small signal-to-noise values. Therefore, even if measurement noise increases after differentiation, the SIDBE algorithm will still work well with the help of ELiS.

Estimation accuracy can be evaluated by testing the residuals of (19) and by means of the deviations of the data from the estimated values, denoted by

$$rs_k = \frac{v_{mk}}{u_{mk}} - \hat{H}(\Omega_k). \tag{23}$$

Also, the confidence intervals of identification can be obtained through standard deviation of the estimated poles and zeros. The sensitivity matrix of zeros and poles on the coefficients of the corresponding polynomials was calculated in [21]. The equation is

$$S(i,j) = \frac{r(i)^j}{\frac{df(r(i))}{dr(i)}} \tag{24}$$

where $r(i)$ is the $i$th root of the polynomial $f(r(j))$. Evaluation of standard deviation uses numerical differentiation in calculating the zero/pole sensitivity to parameter variation. The detailed formulation can be found in [21].

### *C. Identification of Coulomb Friction*

After the linear block is identified, the Coulomb friction can also be determined by means of the following method. After a proper step input is applied to the system, the velocity $v$ will reach a steady state $v_{dc}$ after the transient response is damped out. At this point, if the input to the linear block is $w_{dc}$ and the dc-gain of the linear block is $k_{dc}$, the equation of velocity can be formulated as

$$v_{dc} = w_{dc} \cdot k_{dc} = (u_{dc} - F_c) \cdot k_{dc}. \tag{25}$$

Therefore, the Coulomb friction in the direction of the input force can be derived as

$$F_c = u_{dc} - \frac{v_{dc}}{k_{dc}}. \tag{26}$$

In this way, the Coulomb friction in both directions can be evaluated.

### *D. Identification Procedure*

The SIDBE procedure proposed in this paper is shown in Fig. 10. The steps in the procedure are listed as follows.

1) Design the input excitation $u_1$ with specified frequency contents; then construct $u_2$ with the same frequency components and slightly smaller magnitude.
2) Apply the inputs $u_1$ and $u_2$ to the system and collect the output data $v_1$ and $v_2$, respectively.
3) Transform the collected I/O pairs into the frequency domain and derive the required differential I/O pair, $(u_1 - u_2)$ and $(v_1 - v_2)$.
4) Apply ELiS to perform linear block identification with the differential I/O pair, $(u_1 - u_2)$ and $(v_1 - v_2)$.
5) Determine the Coulomb friction in both directions.
6) Verify the result by means of simulation. If the verification result is not satisfactory, go to Step 2) to increase the excitation magnitude, or go to Step 1) to redesign the excitations with a different frequency spectrum.

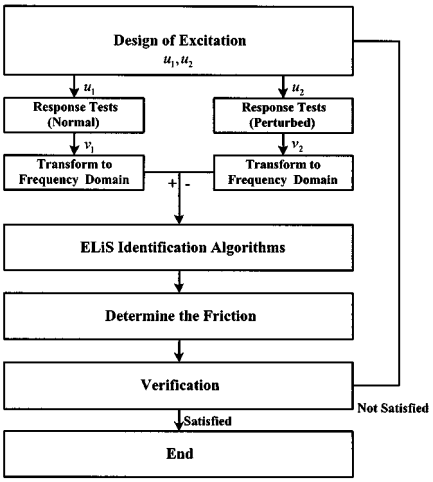


Fig. 11. Proposed SIDBE procedures.

## V. Numerical Investigations

In this section, we will use numerical examples to demonstrate the use of the proposed SIDBE algorithm. Our simulations were coded and run under the MATLAB 5.3 environment from Mathworks. The target system to be identified was that shown in Fig. 5 with a first-order linear block and a nonlinear friction feedback block. The nonlinear block of friction was coded in the C language and compiled to cooperate with the linear system block in Simulink. In real situations, Coulomb friction is often asymmetric. Therefore, its magnitude was assumed to be 0.4 in the negative direction and 0.5 in the positive direction. The linear block is described by a transfer function

$$G(s) = \frac{10}{s+10}. \tag{27}$$

### A. SIDBE Example 1

Following the SIDBE procedure shown in Fig. 11, identification was conducted as follows.

*1) Input Excitation Design:* According to the discussion in the previous section, the excitation signal was designed as a multifrequency binary sequence. Its frequency components included the prime-number (less than 30) multiples of the fundamental frequency $\Delta F$, i.e., $[3, 5, 7, 11, 13, 17, 19, 23, 29] \times \Delta F$, with $\Delta F = 2000/4096 = 0.49$ Hz. Hence, the frequency range was from 1.465 Hz to 14.16 Hz, which was sufficient for our example with a bandwidth of 10 rad/s, i.e., 1.59 Hz.

The harmonic frequencies selected as prime-number multiples of the fundamental frequency prevented the nonlinearity from disturbing the identification procedure. The input and output signals were sampled with a sampling frequency of 2000 Hz. Sampling was synchronized with the excitation signal, so that 4096 samples were taken during each period. The data records contained 8192 points; that is, two periods are measured. For the purpose of comparison, the excitation magnitudes are selected as [1, 1.1, 2, 2.1, 3, 3.1, 4, 4.1, 5, 5.1], ten different values in total. The frequency- and the time-domain components of the magnitude three signal are illustrated in Fig. 12.

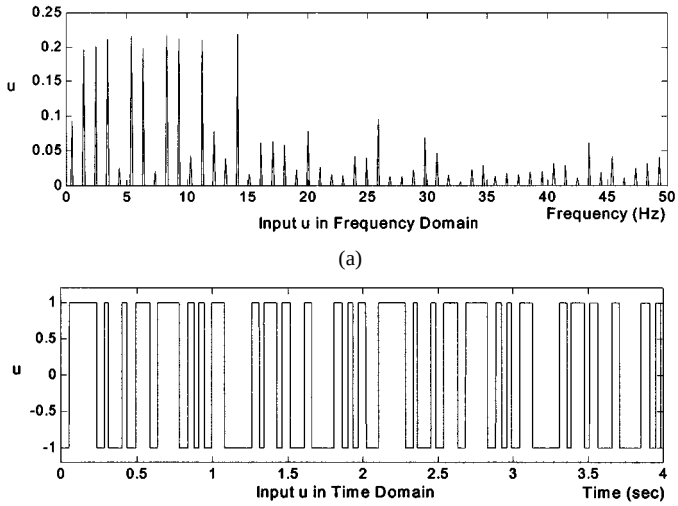


Fig. 12. (a) Input excitation signal in the frequency domain. (b) Input excitation signal in the time domain.

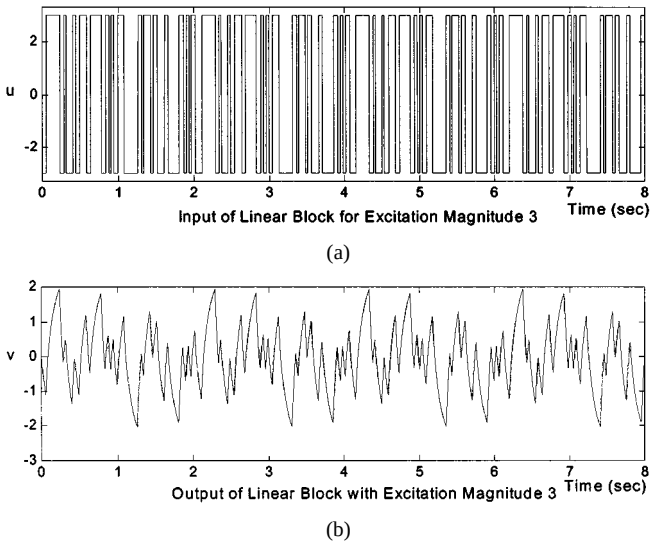


Fig. 13. (a) Input of the linear block for magnitude three excitation. (b) Output of the system with magnitude three excitation.

*2) Output Response Acquisition:* The system was then simulated with the generated excitation signals. The corresponding outputs ($v$) and the inputs of the linear block ($w$) were calculated, respectively, and the responses for magnitude three excitation are shown in Fig. 13.

*3) Data Transformation and Difference Calculation:* Under an input excitation magnitude of 3.1–3, the obtained frequency spectrums for the input ($u_1 - u_2$) and the corresponding output ($v_1 - v_2$) are those shown in Fig. 14.

*4) ELiS System Identification/Coulomb Friction Determination:* With the differential I/O data pair shown in Fig. 14, we proceeded with system identification using the ELiS method. For the purpose of comparison, five models were derived with different magnitudes of differential input excitation.

The parameters for the target plant, including the friction in both directions, are listed in Table I. As the reader can see, the parameters converged to the target value as the input magnitude increased. However, the identified parameters were

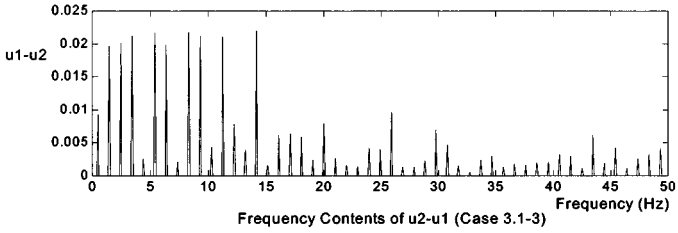


(a)

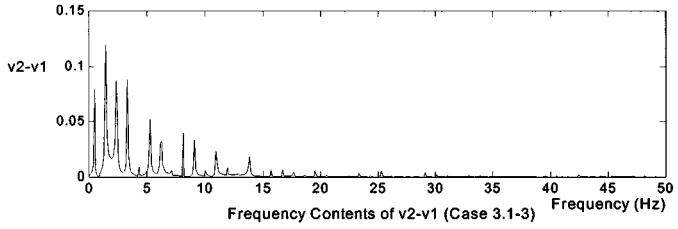


(b)

Fig. 14. Frequency spectrums of (a) $u_1 - u_2$ and (b) $v_1 - v_2$.

TABLE I
SIDBE IDENTIFICATION RESULTS FOR $G(s) = 10/s + 10$ WITH FRICTION

| | Pole | Constant | Dc-gain | $F_c$(+) | $F_c$(-) |
|---|---|---|---|---|---|
| Target | -10 | 10 | 1 | 0.5 | 0.4 |
| 1.1-1 | -14.6441 | 12.5365 | 0.8561 | 0.4159 | 0.2991 |
| 2.1-2 | -10.7959 | 10.5423 | 0.9765 | 0.4880 | 0.3856 |
| 3.1-3 | -10.3117 | 10.2206 | 0.9912 | 0.4955 | 0.3946 |
| 4.1-4 | -10.1429 | 10.1167 | 0.9974 | 0.4987 | 0.3984 |
| 5.1-5 | -10.0687 | 10.0676 | 0.9999 | 0.4999 | 0.3999 |

already within 1% error for the dc gain with an input magnitude of 3.1–3.

### *B. SIDBE Example 2*

Next, we will consider a more complicated example with a 3-pole system that resembles the condition where full position feedback is applied to a servo system. The transfer function is as follows:

$$G(s) = \frac{10\,000}{(s+10)(s^2+5s+1000)}. \tag{28}$$

The dominant poles of the system are two lightly damped conjugate poles. According to [19], the parameters for lightly damped systems are numerically sensitive and are difficult to identify. The results for the identified parameters are listed in Table II. The reader can see that the identification result are very good and are within 1% error for the dc gain at an input magnitude 6.1–6.

To further demonstrate the advantage of our SIDBE method, we repeated the identification procedure using the standard ELiS method but without using differential input excitation. The identification procedure is conducted with input magnitudes of two, four, and six for comparison purposes and the results are shown in Table III.

The identified results are obviously not as good as those for SIDBE identification. The dc gain error for an input magnitude of six is about 10%, compared to 1% in the SIDBE case. Moreover, the ELiS method assumes linearity of the identified plant and is not able to determine the Coulomb friction, while SIDBE can.

TABLE II
SIDBE IDENTIFICATION RESULTS FOR $10\,000/(s+10)(s^2+5s+1000)$ WITH FRICTION

| | Root1 | Root2 | Root3 | Dc-gain | $F_c$(+) | $F_c$(-) |
|---|---|---|---|---|---|---|
| True | -10 | -2.5+31.5238I | -2.5-31.5238I | 1 | 0.5 | 0.4 |
| 1.1-1 | -11.2211 | -1.6418+31.8655I | -1.6418-31.8655i | 0.9030 | 0.4463 | 0.3355 |
| 2.1-2 | -11.6610 | -2.7289+31.6188I | -2.7289-31.6188i | 0.9095 | 0.4503 | 0.3403 |
| 3.1-3 | -11.5791 | -2.7827+31.4247I | -2.7827-31.4247i | 0.9157 | 0.4540 | 0.3448 |
| 4.1-4 | -12.3667 | -2.6973+31.3283I | -2.6973-31.3283i | 0.8661 | 0.4227 | 0.3073 |
| 5.1-5 | -10.2545 | -2.6039+31.4809I | -2.6039-31.4809i | 0.9830 | 0.4913 | 0.3896 |
| 6.1-6 | -10.1138 | -2.5714+31.5253I | -2.5714-31.5253i | 0.9903 | 0.4951 | 0.3941 |

TABLE III
ELiS IDENTIFICATION RESULTS FOR $10\,000/(s+10)(s^2+5s+1000)$ WITH FRICTION

| | Root1 | Root2 | Root3 | Dc-gain | $F_c$(+) | $F_c$(-) |
|---|---|---|---|---|---|---|
| True | -10 | -2.5+31.5238I | -2.5-31.5238I | 1 | 0.5 | 0.4 |
| 2 | -11.7107 | -1.3509 +31.9106I | -1.3509 -31.9106i | 0.8511 | - | - |
| 4 | -11.5258 | -1.9065 +31.6720I | -1.9065 -31.6720i | 0.8859 | - | - |
| 6 | -11.3114 | -2.1197 +31.5919I | -2.1197 -31.5919i | 0.9046 | - | - |

TABLE IV
COMPARISON OF RESULTS OBTAINED USING ELiS AND LS

| | Root1 | Root2 | Root3 | Dc-gain | $F_c$(+) | $F_c$(-) |
|---|---|---|---|---|---|---|
| Target | -2.5-31.5238I | -2.5+31.5238I | -10 | 1 | 0.5 | 0.4 |
| ELiS:1.1-1 | -1.9019-32.2174I | -1.9019+32.2174I | -11.373 | 0.90926 | 0.4501 | 0.34012 |
| LS:1.1-1 | -1.6766-32.8873I | -1.6766+32.8873I | -9.9403 | 0.91695 | 0.45472 | 0.34566 |
| ELiS:2.1-2 | -2.5026-31.8556I | -2.5026+31.8556I | -11.125 | 0.93261 | 0.46387 | 0.35665 |
| LS:2.1-2 | -2.324-32.0724I | -2.324+32.0724I | -10.321 | 0.93946 | 0.46778 | 0.36133 |
| ELiS:3.1-3 | -2.5752-31.7020I | -2.5752+31.7020I | -11.036 | 0.9444 | 0.47056 | 0.36468 |
| LS:3.1-3 | -2.4035-31.8404I | -2.4035+31.8404I | -10.344 | 0.95138 | 0.47445 | 0.36934 |
| ELiS:4.1-4 | -2.5834-31.6226I | -2.5834+31.6226I | -11.331 | 0.92079 | 0.45699 | 0.34838 |
| LS:4.1-4 | -2.3934-31.7484I | -2.3934+31.7484I | -10.411 | 0.95432 | 0.47607 | 0.37128 |
| ELiS:5.1-5 | -2.558-31.6727I | -2.558+31.6727I | -10.308 | 0.99521 | 0.4976 | 0.39712 |
| LS:5.1-5 | -2.3776-31.7686I | -2.3776+31.7686I | -9.9197 | 0.9901 | 0.4950 | 0.3940 |

The above examples without the noise effect have demonstrated the improvement that can be achieved using SIDBE compared with the conventional method. Next, we will introduce noise to corrupt I/O data and further study SIDBE performance under this condition.

In the test, the commonly applied time-domain least-square (LS) estimator [3], [22] was compared with SIDBE. In the time domain, the LS estimator estimated the target plant, formulated as an ARX model. The identified parameters were then transformed to the $s$-domain for the purpose of comparison. Two white noise signals with zero mean and 0.1 variances were then added to corrupt the input and output measurements and the results are shown in Table IV.

In all cases shown above, ELiS is competitive with LS. The maximum likelihood (ML) estimator for a model linear in terms of parameters and with normally distributed white noise is identical to the Markov estimator. In the case of disturbance with the covariance matrix $\sigma^2 I$, it follows that the ML estimator reduces to the LS estimator [3].

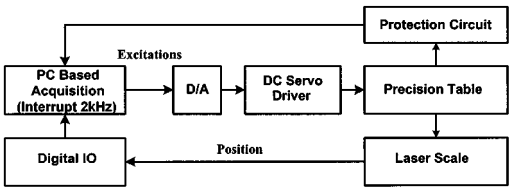


Fig. 15. Block diagram of the experimental system.

Fig. 16. Precision ball–crew table with laser scale.

TABLE V
SPECIFICATIONS OF THE TABLE

| | |
|---|---|
| **Stroke** | $200mm$ |
| **Pitch** | $2mm$ |
| **Repeatability** | $0.001mm$ |
| **Backlash** | $0.001mm$ |
| **Laser Scale Resolution** | $10nm$ |

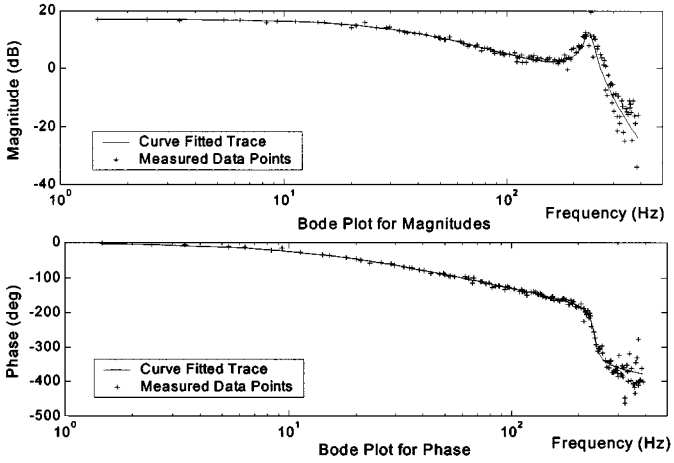


Fig. 17. Bode plot for the precision table (with an excitation magnitude of 520–510).

## VI. EXPERIMENT

We shall apply the proposed SIDBE method to identify the model of a precision positioning system in this section. At first, we will start with the system setup and then we will present the experimental results, which are very satisfying.

### A. Apparatus

The system setup basically consists of a precision ball–screw system with drivers and amplifiers, a laser scale, a digital I/O interface, protection circuits and a PC-based controller. The block diagram is depicted in Fig. 15.

*NSK Ball–Screw:* The main component of our positioning system is a precision ball–screw table made by NSK Inc., Japan, which is driven by a dc motor with low-noise linear amplifiers. The whole setup is fixed to a granite stone plate with a vibration-resistance table, as shown in Fig. 16. The specifications of the table are listed in Table V.

*Sony Laser Scale:* High-precision control always depends on high-resolution sensors for obtaining position feedback. Stable and reliable position sensors are usually required. Laser interferometers and scales are popular high-precision sensing devices due to their advantages of measurement stability and accuracy. Our high-precision ball–screw table is equipped with a SONY 10-nm laser scale for full position feedback. With the help of the SONY laser scale, the resolution of the table reaches the submicrometer level.

*Protection Circuit:* In order to protect these high-precision devices, a specially designed logic circuit and limit switches have been added at both ends of the table. Once the moving table reaches the limits at both sides, the protection circuit cuts off the power and stops the dc motors, thus preventing further movement.

*Data Acquisition and Interfaces:* A Pentium-based personal computer equipped with an interface card is used as the controller of the system. The data acquisition program is implemented in the C language under the MS-DOS environment and is coded as an interrupt that is triggered by a timer with a frequency of 2000 Hz.

### B. Experimental Results

In this section, we will discuss the experimental procedures and present results for identification of the precision table.

*Design of Excitation Signal:* Following the above discussion, the test signals were constructed with frequency contents of [3, 5,..., prime numbers less than 700] $\times \Delta F$, with $\Delta F = 2000/4096 = 0.49$ Hz. Consequently, the range of the frequency contents was about 1.465 Hz–389.16 Hz, which should be appropriate for most mechanical systems with bandwidths of, at most, tens of hertz. The constructed signal stream was a periodic signal consisting of 4096 points in one period, repeated for five periods of time with a total of 20 480 samples.

The digital to analog interface used in the experiment was of 12 bits and the output level was $\pm 10$ V, i.e., $+2048$ corresponding to $+10$ V and $-2048$ to $-10$ V. For convenience and clarity, the output level is temporarily represented here by D/A counts instead of volts.

*SIDBE Identification:* SIDBE identification was applied with two different excitation magnitudes of 520 and 510. The ELiS algorithm comes up with a 5-pole model. The Bode plot of the identified model is shown in Fig. 17. The "+" marks stand for the measured values at each predefined frequency point and the solid line represents the curve fitted model derived using the ELiS method. Fig. 17 shows that the model fits quite well at low frequencies up to about 200 Hz.

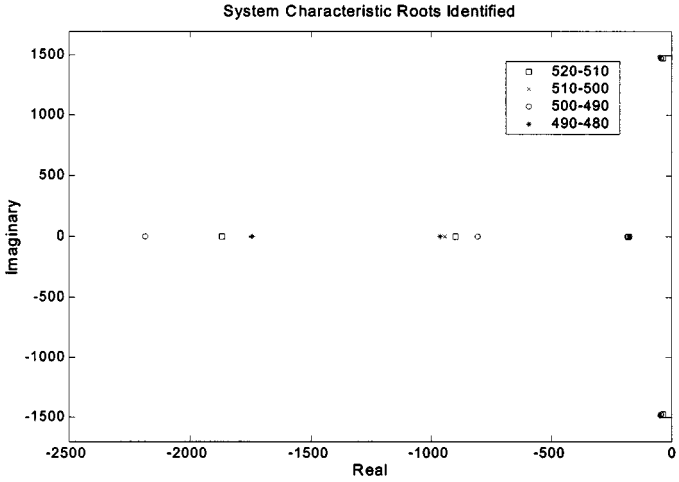


Fig. 18. Identified characteristic roots of models (□: 520–510 D/A counts, ×: 510–500, ○: 500–490, and ·×·: 490–480).

TABLE VI
VALUES FOR IDENTIFIED CHARACTERISTIC ROOTS OF MODELS

| | Root1 | Root2 | Root3 | Root4 | Root5 | Dc-gain |
|---|---|---|---|---|---|---|
| 520-510 | -1868.5 | -900.2 | -179.8 | -37.7+1478.9I | -37.7-1478.9i | 6.9931 |
| | std:44.6208 | 16.4458 | 0.9902 | 0.9425+1.5821I | 0.9425+1.5821I | |
| 510-500 | -1754.3 | -945.9 | -178.5 | -46.8+1478.3I | -46.8-1478.3i | 6.9921 |
| | 51.0870 | 21.4549 | 0.9744 | 1.1754+1.4470I | 1.1754+1.4470I | |
| 500-490 | -2185.5 | -805.9 | -183.7 | -46.0+1476.6I | -46.0-1476.6i | 6.9879 |
| | 45.7844 | 11.6445 | 1.0559 | 0.9447+1.2063I | 0.9447+1.2063I | |
| 490-480 | -1744.1 | -963.5 | -173.2 | -50.2+1490.9I | -50.2-1490.9i | 7.1201 |
| | 48.8653 | 21.5668 | 0.9145 | 0.9856+1.2264I | 0.9856+1.2264I | |
| Mean | -1888.1 | -903.9 | -178.8 | -45.1+1481.2I | -45.1-1481.2i | 7.0233 |

The peak in the bode plot indicates that the system has lightly damped poles, derived at $-37.7+1478.9i$ and $-37.7-1478i$, respectively.

To further investigate the precision table, three more experiments were conducted with different magnitudes of input excitation. The five poles in each model are plotted in Fig. 18 and listed in Table VI for comparison.

The poles shown in Fig. 18 are separated into five groups with two conjugate poles near the imaginary axis. The conjugate poles provide information about the natural frequency of the system. Further, one can see a group of poles centered around $-180$ on the real axis. The above three groups of dominant poles are quite consistent for all four identifications, whereas the other two groups of poles at higher frequencies are not as close to one another.

Finally, the overall plant model was determined by computing the geometric means in each group of poles. The confidence interval is indicated by the standard deviation [see (24)], for each pole, which is listed below the value of the corresponding root. When the pole value was complex, standard deviations for both the real and imaginary parts were calculated. The detailed results are listed in Table VI.

Hence, the linear model in the $s$-domain is

$$G(s) = \frac{4.69\cdot 10^{15}}{s^5+3061s^4+4.67\cdot 10^6 s^3+7.03\cdot 10^9 s^2+4.87\cdot 10^{12}s+6.70\cdot 10^{14}} \cdot \text{mm/s}\cdot\text{V}. \quad (29)$$

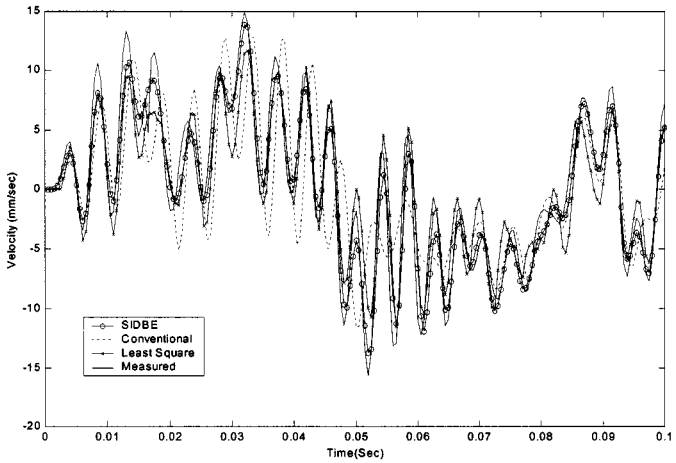


Fig. 19. Comparison of results for SIDBE and the other identification algorithms under PRBS input (SIDBE: solid line with circles; LS: solid line with crosses; conventional method: dashed line; measured data: solid line).

Friction was determined by first applying a command of 1500 D/A counts (7.32 V) to the motor driver. Then, the steady-state velocity was measured and found to be 41.9 mm/s in the positive direction. The output polarity was then reversed and the steady-state velocity measured and found to be 39.5 mm/s. Following the discussions in Section IV, the Coulomb friction in the positive direction was found to be 1.33 V and in the negative direction was calculated as 1.67 V using (26).

*Model Verification:* Without knowing the true plant parameters, we could not verify the superiority of the identified models. To verify the identified system model, another test excitation was created and the corresponding output was measured. The test excitation was generated from the pseudorandom binary sequence (PRBS). The measured PRBS output trace was chosen as the basis for comparison. To make a comparison, the previously identified models were all simulated with the new test excitation. The simulated results together with the measured PRBS output are shown and compared in Fig. 19.

In Fig. 19, the solid line represents the true measured PRBS output. The solid line with circles indicates the results for the SIDBE identified model, the solid-line with crosses denotes the results for the time-domain LS method and the dotted line indicates the results for the standard ELiS algorithm without differential input excitations. Fig. 20 shows the relative error based on the measured PRBS for different identification algorithms. From Fig. 20, it is clear that the SIDBE algorithm successfully obtained the behaviors of the precision table with an error level smaller than that for LS and the standard ELiS case.

### C. Discussion

Possible sources of the modeling errors are measurement noise, position-dependent friction, and unmodeled high-frequency dynamics. The friction model in SIDBE was assumed to be position-independent. However, in reality, the friction in a ball–screw table is naturally position-dependent. Due to the rotating motion of the ballscrew, the friction force of the precision table is periodic and position-dependent. Moreover,

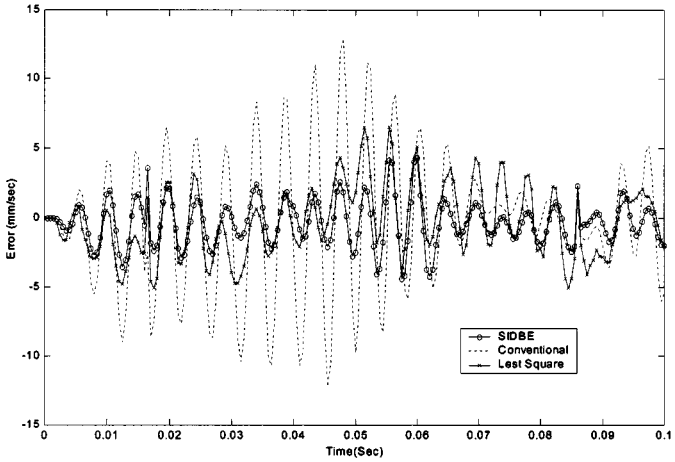


Fig. 20. Estimation errors corresponding to measured data in the time domain (SIDBE error: solid line with circles; LS error: solid line with crosses; conventional method error: dashed line).

the period of friction is equal to the length of the ball–screw pitch [20]. The changing friction effect is not considered in our identification algorithm, which also contributes to the modeling error.

Usually, increasing the order of the identified model can reduce the modeling error due to unmodeled dynamics at high frequencies. However, a tradeoff will appear in the later controller design stage. Whether or not to increase the order of the identified model, therefore, depends on the expected working frequency span of the identified system.

## VII. Conclusion

A system identification algorithm, SIDBE, has been developed and successfully applied to a precision servo system with intrinsic friction. The key feature that distinguishes SIDBE from conventional frequency-domain identification is the design of the differential binary excitation. A typical servo system with Coulomb friction usually takes the form shown in Fig. 4. In order to derive an accurate model of the linear block as well as the Coulomb friction, it is crucial to decouple the linear part from the nonlinear feedback friction. In addition, the behavior of the Coulomb friction can be greatly simplified and the stick phenomenon avoided if constant excitation with a magnitude larger than the maximum static friction is applied. Moreover, the difference between two similar input excitations is observed to be almost identical to the difference between the corresponding input excitations to the linear block. It is, therefore, obvious that the differential I/O pairs should be employed in linear block identification.

SIDBE has been shown to be extremely useful for the identification of servo systems with friction. Experiments have been conducted involving identification of a linear model of a precision ball–screw system with associated Coulomb friction. The identified model has been shown to accurately match the experimental data as shown in Fig. 18. Furthermore, our approach can be extended to similar physical systems having the same nonlinear property. With proper modification, it can be adapted to more complex situations in frequency response analysis.

## References

[1] L. A. Zadeh, "From circuit theory to system theory," *Proc. IRE*, vol. 50, pp. 856–865, 1962.
[2] K. Ogata, *Modern Control Engineering*. Englewood Cliffs, NJ: Prentice-Hall, 1990.
[3] R. Johansson, *System Modeling and Identification*. Englewood Cliffs, NJ: Prentice-Hall, 1993.
[4] B. Armstrong-Hélouvry, P. Dupont, and C. Canudas de Wit, "A survey of models, analysis tools and compensation methods for the control of machines with friction," *Automatica*, vol. 30, no. 7, pp. 1083–1138, 1994.
[5] C. Canudas de Wit and J. Carillo, "A weighted RLS algorithm for systems with bounded disturbances," in *Proc. IFAC Conf. Identification Syst. Parameter Identification*, Beijing, P. R. China, 1988, pp. 879–884.
[6] B. V. Derjaguin, V. E. Push, and D. M. Tolstoi, "A theory of stick-slip sliding of solids," in *Proc. Conf. Lubrication Wear*, London, U.K., 1957, pp. 257–268.
[7] M. R. Elhami and D. J. Brookfield, "Sequential identification of coulomb and viscous friction in robot drives," *Automatica*, vol. 33, no. 3, pp. 393–401, 1997.
[8] C. Canudas de Wit, K. J. Åström, and K. Braun, "Adaptive friction compensation in DC motor drives," *IEEE J. Robot. Automat.*, vol. RA-3, Nov. 1987.
[9] E. D. Tung and M. Tomizuka, "Feedforward tracking controller design based on the identification of low frequency dynamics," *ASME J. Dynamic Syst., Meas., Contr.*, vol. 115, pp. 348–356, 1993.
[10] H. S. Lee and M. Tomizuka, "Robust high-speed servo-controllers for micropositioning system," in *Proc. 3rd Int. Workshop Advanced Motion Contr.*, Berkeley, CA, 1994, pp. 633–642.
[11] J. H. Kim, H. K. Chae, J. Y. Jeon, and S. W. Lee, "Identification and control of systems with friction using accelerated evolutionary programming," *IEEE Contr. Syst. Mag.*, pp. 38–47, Aug. 1996.
[12] B. Armstrong-Hélouvry and B. Amin, "PID control in the presence of static friction: A comparison of algebraic and describing function analysis," *Automatica*, vol. 32, no. 5, pp. 679–692, 1996.
[13] A. van den Bos and R. G. Krol, "Synthesis of discrete-interval binary signals with specified fourier amplitude spectra," *Int. J. Contr.*, vol. 30, no. 5, pp. 871–884, 1979.
[14] K. D. Paehlike and H. Rake, "Binary multifrequency signals-synthesis and application," in *Proc 5th IFAC Symp. Identification Syst. Parameter Estimation*, vol. 1, 1979, pp. 589–596.
[15] C. Evams, D. Rees, and D. L. Jones, "Identifying linear models of systems suffering nonlinear distortions, with a gas turbine application," *Proc. Inst. Elect. Eng. Contr. Theory Applicat.*, vol. 142, no. 3, pp. 229–240, 1995.
[16] J. G. Mueller, B. A. A. Antao, and R. A. Saleh, "A multifrequency technique for frequency response computation with application to switched-capacitor circuits with nonlinearities," *IEEE Trans. Comput.-Aided Design*, vol. 15, pp. 775–790, July 1996.
[17] I. Kollár, "On frequency domain identification of linear systems," *IEEE Trans. Instrum. Meas.*, vol. 42, pp. 2–6, Jan. 1993.
[18] R. Pintelon and J. Schoukens, "Robust identification of transfer functions in s- and z-domain," *IEEE Trans. Instrum. Meas.*, vol. 33, pp. 565–573, July 1990.
[19] D. S. Bayard, "High-order wide-band frequency domain identification using composite curve fitting," in *Proc. Amer. Contr. Conf.*, 1992, pp. 3181–3185.
[20] P. Y. Huang, Y. Y. Chen, and M. S. Chen, "Position-dependent friction compensation for ballscrew tables," in *Proc. IEEE Int. Conf. Contr. Applicat.*, Trieste, Italy, 1998, pp. 863–867.
[21] P. Guillaume, J. Schoukens, and R. Pintelon, "Sensitivity of roots to errors in the coefficients of polynominals obtained by frequency-domain estimation methods," *IEEE Trans. Instrum. Meas.*, vol. 38, pp. 1050–1056, Nov. 1989.
[22] K. Kozlowski, *Modeling and Identification in Robotics*. New York: Springer-Verlag, 1998.

**Yung-Yaw Chen** (S'87-M'89) received the B.S. degree in electrical engineering from National Taiwan University, Taipei, Taiwan, in 1981 and the Ph.D. degree in electrical engineering and computer science from University of California at Berkeley, Berkeley, in 1989.

He is a Professor at the Department of Electrical Engineering, National Taiwan University, where he does research on intelligent control, fuzzy logic, computational intelligence, precision servo control, and hyperthermia treatment planning. He has published more than 100 papers, including 30 journal papers in these areas. He also serves as an Associate Editor of the *International Journal of Fuzzy Systems*.

Dr. Chen received the Excellent Research Awards from the National Science Council in 1990 and 1991. He was the Program Chair in 1996 of Asian Fuzzy Systems Symposium and Vice Program Chair of the 2000 IFSA Conference. He is a member of the IEEE Control Systems Society, Computer Society, Neural Networks Society, Systems, Man and Cybernetics Society, and Ultrasound Society.

**Pai-Yi Huang** was born in Changhua, Taiwan. He received the B.E. degree in power mechanical engineering from National Tsing Hua University, China, in 1992 and the Ph.D. degree in electrical engineering from National Taiwan University, Taipei, Taiwan, in 2000.

From 1993 to 1996, he was a Researcher with the Advanced Precision Control Laboratory of the Yen-Tjing-Ling Industrial Research Institute, National Taiwan University, Taiwan. From 1996 to 1998, he served as a Consultant for the Center for Measurement Standards of Industrial Technology Research Institute, Taiwan. His research interests include digital servo control system, precision positioning, and intelligent control. He is currently a BIOS engineer with ASUSTek Computer, Inc.

Dr. Huang is a Member of the Phi Tau Phi scholastic honor society.

**Jia-Yush Yen** received the B.S. degree from National Tsing-Hwa University, Taipei, Taiwan, in 1980, the M.Sc. degree from University of Minnesota, Minneapolis, in 1983, and the Ph.D. degree from University of California at Berkeley, Berkeley, in 1989, all in mechanical engineering.

Since then, he has been with National Taiwan University, where he is currently a Professor of Mechanical Engineering. He has served as a Consultant for many companies. His research interests include mechatronic systems, computer peripherals, and micromechanical systems.

Dr. Yen is the treasurer of the Control System Chapter in IEEE Taipei Section in 1994. He is a Member of the ASME.